

Simplified Optimization Model for Low-Thrust Perturbed Rendezvous Between Low-Eccentricity Orbits

An-yi Huang^{a,*}, Heng-nian Li^a

^aState Key Laboratory of Astronautic Dynamics, Xi'an 710043, China

Received ; Received in final form ; Accepted ;
Available online

Abstract

Trajectory optimization of low-thrust perturbed orbit rendezvous is a crucial technology for space missions in low Earth orbits, which is difficult to solve due to its initial value sensitivity, especially when the transfer trajectory has many revolutions. This paper investigated the time-fixed perturbed orbit rendezvous between low-eccentricity orbits and proposed a priori quasi-optimal thrust strategy to simplify the problem into a parametric optimization problem, which significantly reduces the complexity. The optimal trajectory is divided into three stages including transfer to a certain intermediate orbit, thrust-off drifting and transfer from intermediate orbit to the target orbit. In the two transfer stages, the spacecraft is assumed to use a parametric law of thrust. Then, the optimization model can be then obtained using very few unknowns. Finally, a differential evolution algorithm is adopted to solve the simplified optimization model and an analytical correction process is proposed to eliminate the numerical errors. Simulation results and comparisons with previous methods proved this new method's efficiency and high precision for low-eccentricity orbits. The method can be well applied to preliminary analysis and high-precision trajectory optimization of missions such as in-orbit service and active debris removal in low Earth orbits.

© 2022 All rights reserved.

Keywords: Low-thrust perturbed rendezvous; Trajectory optimization; Parametric optimization model; Numerical error correction

1. Introduction

Trajectory optimization of perturbed orbit rendezvous is a crucial technology for space missions in low Earth orbits (LEOs) (Bonnal et al., 2013; Shen & Tsiotras, 2005). Low-thrust electrical propulsion is usually preferred in such missions because of its high efficiency (Moghaddam & Chhabra, 2021; Ruggiero et al., 2015; Leomanni et al., 2020). As the thrust is insignificant compared with the Earth's gravity, the transfer trajectory usually has many revolutions, which brings additional

difficulty for trajectory optimization. In this condition, existing numerical methods (Jiang et al., 2012; Li et al., 2018; Zhao et al., 2017; Guo et al., 2018; Neves & Sanchez, 2020) are very sensitive to the initial values in the shooting process and thus easily converge to local solutions of different revolutions. Moreover, the numerical orbit propagation including the non-linear perturbations is also time-consuming when the transfer duration is very long. Averaging methods (Gao, 2007; Tarzi et al., 2013; Kelchner & Kluever, 2020; Pontani & Pustorino, 2021) can be applied to replace the time-consuming orbit calculation. However, special assumptions are required and it's hard to find a general optimization method applicable for all type of orbits.

This paper mainly studies the fuel-optimal trajectory opti-

*Engineer, Xi'an Satellite Control Center. hay04@foxmail.com

*Corresponding author: Tel.: +8684762399; fax: +8684762399;

¹Professor, Xi'an Satellite Control Center.

mization of time-fixed orbit rendezvous in LEOs with low eccentricity. The major effect of the perturbations on a spacecraft is from the J_2 term of the Earth's non-sphere perturbation, which drifts the rising node right ascension (RAAN) and the argument of perigee with constant velocities (P, 2004). Therefore, instead of correcting the derivations brought by J_2 perturbation, one can utilize the natural drift of orbit elements actively to save the propellant.

Several studies simplified the problem to quickly evaluate the approximate propellant consumption for mission analysis and the global optimization of multi-target rendezvous problems. Cerf (2014) analyzed the feasibility of actively changing the semimajor axis and inclination to use the natural drift of the right ascension of ascending node and reduce the propellant and studied its application in target selection for an active debris removal mission. Berend & Olive (2016) discretized the semimajor axis and inclination to search for an optimal RAAN drift rate, which can partly reduce the complexity of global optimization. Shen (2021) established an approximate model of low-thrust orbit rendezvous for circular orbits and derived the analytical expression of velocity increment. Huang et al. (2020, 2022a) proposed an equality constraint optimization model of impulsive rendezvous and designed an iterative method to expand the impulsive solution to an equivalent low-thrust solution with high precision for orbits with small eccentricity. However, these methods cannot obtain the law of thrust and transfer trajectory.

To obtain the approximate thrust law, Cerf (2016) proposed an optimization model that only considered semimajor axis, inclination, and RAAN based on the minimum principle. Wen et al. (2021) improved Cerf's method by introducing the yaw switch strategy and reduced the propellant consumption in some cases. Such idea could be also found in (Barea et al., 2022; Casalino & Forestieri, 2022). These methods introduced an intermediate drift orbit and let the spacecraft transfer to the drift orbit using Edelbaum's time-optimal strategy (Edelbaum, 2003). As an improvement, Huang et al. (2022b) designed a parametric thrust strategy that allows the thrust to periodically switch between on and off when transferring to the drift orbit. Then, an equality constraint optimization model can be obtained and quickly solved. Moreover, in (Huang et al., 2022b), an analytical correction process was introduced to obtain the high-precision trajectory that considered full perturbations. These methods can only adapt to circular orbits. However, most of the debris and satellites in LEO are in elliptical orbits of small eccentricities, which should be considered in trajectory optimization. Therefore, this study investigates the fast optimization model of low-thrust rendezvous between elliptical orbits.

We propose a novel simplified parametric thrust strategy to approximate the optimal control law for fuel-optimal low-thrust rendezvous between low-eccentricity orbits, significantly improving the efficiency of the trajectory optimization. The major contribution can be summarized as three points:

(1) Based on the three-stages near-optimal strategy for rendezvous with circular orbits (Huang et al., 2022b), an approximate optimization model including the radial component

of thrust and allowing the length of two thrust-on arcs of each revolution to be asymmetric is proposed in this study. Thus, the obtained trajectory could satisfy the constraints on the six-dimensional orbit elements.

(2) A fast solving process to judge the feasibility of a low-thrust single-revolution transfer and obtain the thrust parameters is proposed to reduce the dimensionality of the optimization model and improve the efficiency.

(3) A fast analytical correction process is proposed to obtain high-precision trajectory using the numerical errors between predicted orbit and target orbit.

Simulation results proved that the proposed method could quickly obtain the optimal high-precision transfer trajectory. The calculation is much smaller than indirect methods that often obtain local optimal solutions and thus need to repeat the shooting process with different initial values of costate for selecting the best solution. Compared with existing approximate methods, the proposed parametric optimization method considers constraints on eccentricity and is more precise for elliptical orbits.

2. Problem description

This study focuses on the fuel-optimal trajectory of time-fixed orbital rendezvous. Assuming $\sigma_0 = [a_0, e_0, i_0, \Omega_0, \omega_0, M_0]$ represents the initial orbit elements (a: semimajor axis, e: eccentricity, i: inclination, Ω : RAAN, ω : argument of perigee, M: mean anomaly, and subscript '0' means initial orbit) for the spacecraft at t_0 and $\sigma_f = [a_f, e_f, i_f, \Omega_f, \omega_f, M_f]$ (subscript 'f' means target orbit) presents the target orbit elements at t_f , the trajectory optimization is a typical optimal control problem that need to solve the optimal thrust acceleration $\alpha(t)$ that satisfy the terminal constraint and minimize the propellant cost. Let $\sigma(t) = [a, e, i, \Omega, \omega, M]$ denote the orbit elements during the transfer, the dynamics equations are

$$\begin{cases} \frac{da}{dt} = \frac{2}{n\sqrt{1-e^2}} [(\alpha_r + \alpha_r^{J_2})e \sin f + (\alpha_t + \alpha_t^{J_2})(1 + e \cos f)] \\ \frac{de}{dt} = \frac{\sqrt{1-e^2}}{na} [(\alpha_r + \alpha_r^{J_2}) \sin f + (\alpha_t + \alpha_t^{J_2})(\cos E + \cos f)] \\ \frac{di}{dt} = \frac{r \cos u}{na\sqrt{1-e^2}} (\alpha_n + \alpha_n^{J_2}) \\ \frac{d\Omega}{dt} = \frac{r \sin u}{na\sqrt{1-e^2} \sin i} (\alpha_n + \alpha_n^{J_2}) \\ \frac{d\omega}{dt} = \frac{\sqrt{1-e^2}}{nae} [-(\alpha_r + \alpha_r^{J_2}) \cos f + (\alpha_t + \alpha_t^{J_2})(1 + \frac{r}{p}) \sin f] - \cos i \frac{d\Omega}{dt} \\ \frac{dM}{dt} = n - \frac{1-e^2}{nae} [(\alpha_r + \alpha_r^{J_2})(2e \frac{r}{p} - \cos f) + (\alpha_t + \alpha_t^{J_2})(1 + \frac{r}{p}) \sin f] \end{cases} \quad (1)$$

where f is the true anomaly, $p = a(1 - e^2)$ is the semi-latus rectum, u is the argument of latitude, $n = \sqrt{\frac{\mu}{a^3}}$ is the orbital angular velocity, and $\alpha^{J_2} = [\alpha_t^{J_2}, \alpha_n^{J_2}, \alpha_r^{J_2}]$ are the three acceleration components due to the J_2 perturbation in the local vertical/local horizontal (LVLH) reference frame. $\alpha_t = c(t)\alpha \cos \beta$, $\alpha_n = c(t)\alpha \sin \beta \cos \phi$ and $\alpha_r = c(t)\alpha \sin \beta \sin \phi$ are the three components of $\alpha(t)$ in the LVLH reference frame, where β is the angle between $\alpha(t)$ and the tangential direction, ϕ is the angle between the projection of $\alpha(t)$ in the normal-radial plane and the radial direction, $\alpha = \frac{F_{\max}}{m}$ is the max acceleration expressed by the maximum thrust F_{\max} and mass m , and $c(t) \in [0, 1]$ is engine throttling function representing magnitude of the thrust acceleration.

The objective function can be written as

$$J = \dot{m} \int_{t_0}^{t_f} c(t) dt \quad (2)$$

where $\dot{m} = \frac{F}{I_{sp}g}$ is the constant mass flow rate, I_{sp} is the constant specific impulse, and g is the standard gravitational acceleration at sea level (9.80665 m/s²).

In this study's investigation, when the propellant cost is small compared to the mass (for example, when $I_{sp} = 1000$ s and $\Delta v = 200$ m/s, the fuel cost is approximately 2%), it can be supposed that the mass is constant during the orbit transfer. Then, we can let $\alpha = \frac{F_{max}}{m_0}$ denote the maximum acceleration (m_0 is the initial mass). Since α is much smaller than the Earth's gravity, completing the orbit rendezvous requires a long time. The number of orbit revolutions would be significant, and the orbit propagation would be time-consuming. In the next section, a simplified thrust strategy will be proposed to express $c(t)$, $\beta(t)$, and $\phi(t)$ by a few parameters to reduce the complexity.

3. Methodology

This section first designs a parametric thrust strategy for orbit rendezvous with elliptical orbit and then establishes the simplified optimization model. A sub boundary value problem that solves the optimal parameters corresponding to orbital element changes in a single revolution is embedded in the optimization model to resolve terminal constraints. Finally, a differential evolution algorithm is employed to solve the optimal trajectory.

3.1. Near-optimal thrust strategy

A near-optimal thrust strategy (Huang et al., 2022b) is proposed for transfer between circular orbits and has shown to be efficient. It divides the transfer duration into three stages: transfer to arrive at an intermediate orbit with certain RAAN drift, natural drift duration with no thrust, and transfer from intermediate orbit to the target orbit. Thus, most of the non-coplanar maneuvers required for RAAN control can be avoided with the help of natural RAAN drift caused by J₂ perturbation. In the first and third stages, it's assumed that the near-optimal Bang-Bang control law switches the thrust on and off periodically in each revolution. When the thrust is on, its direction is assumed to be fixed in the LVLH reference frame. Then, the low-thrust optimization problem is simplified using very few parameters (Huang et al., 2022b).

In this study, to satisfy the eccentricity constraints for orbit rendezvous, we expand the thrust strategy by including the radial thrust component to change the eccentricity jointly with the tangential component. As illustrated in Fig. 1, there are two thrust arcs in each revolution, and their middle points are symmetric. When the thrust is on, the acceleration keeps the maximum value. The lengths of the two arcs could not be equal to change eccentricity by the tangential component of thrust while keeping the semimajor axis unchanged. Let u and

$u + \pi$ denote the arguments of altitude, and πk_1 and πk_2 denote the lengths of the two arcs. The three thrust components are fixed (β and ϕ are constant) in the LVLH reference frame, and the values of radial and normal components are opposite in the two arcs. The sign of the tangential components may be the same or opposite, which is expressed by the unknown coefficient $\eta = -1$ or 1 . Then, the trajectory of one revolution can be determined using the six parameters η, k_1, k_2, u, β , and ϕ .

Then, based on the three-stage near-optimal thrust strategy

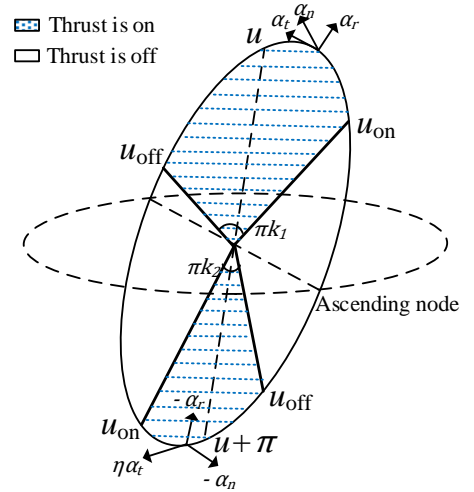


Fig. 1. Fixed thrust strategy in one revolution.

(Huang et al., 2022b) and the improvement above for eccentricity control, the whole transfer trajectory can be expressed by 14 parameters: Δt_1 and Δt_2 denote the duration of the first and third stages; $\eta_1, k_{11}, k_{12}, u_1, \beta_1$, and ϕ_1 denote the parameters of thrust in the first stage (using additional subscript '1'); and $\eta_2, k_{21}, k_{22}, u_2, \beta_2$, and ϕ_2 denote the parameters of thrust in the third stage (using additional subscript '2'). The parametric orbit rendezvous problem is detailed in the following subsections.

3.2. Assumptions declaration

To obtain a simplified model, several assumptions should be declared.

(1) First, the initial and target orbits are near-circular orbits, and $p \approx a \approx r$. In addition, the changes in the semimajor axis and inclination are small enough, thus the a , i , and n in the right function of Eq. (1) are approximately constant and equal to their initial values a_0 , i_0 and n_0 .

Here, dt in Eq. (1) can be replaced by $du = n_0 dt$ because n is also near constant. e and ω are replaced by $e_x = e \cos \omega$ and $e_y = e \sin \omega$ to avoid a singularity. Then, Eq. (1) can be divided into two independent parts: effects of thrust and J₂ perturbation. The changes in orbit elements by the thrust (without

perturbation) are:

$$\begin{cases} \frac{da}{du} = \frac{2a_0\alpha \cos\beta}{n_0V_0} \\ \frac{di}{du} = \frac{\alpha \sin\beta \cos\phi \cos u}{n_0V_0} \\ \frac{d\Omega}{du} = \frac{\alpha \sin\beta \cos\phi \sin u}{n_0V_0 \sin i} \\ \frac{de_x}{du} = \frac{\alpha}{n_0V_0} (2 \cos\beta \cos u - \sin\beta \sin\phi \sin u) \\ \frac{de_y}{du} = \frac{\alpha}{n_0V_0} (2 \cos\beta \sin u - \sin\beta \sin\phi \cos u) \end{cases} \quad (3)$$

where $V_0 = n_0a_0$ is the mean orbital velocity.

The effect of J_2 perturbation is expressed by the analytical form in (Vallado, 2007) as follows:

$$\begin{cases} \frac{da}{dt} = 0 \\ \frac{di}{dt} = 0 \\ \frac{d\Omega}{dt} = -\frac{3J_2n_0r_E^2 \cos i_0}{2a_0^2} \\ \frac{de_x}{dt} = -e \sin \omega \frac{d\omega}{dt} \\ \frac{de_y}{dt} = e \cos \omega \frac{d\omega}{dt} \\ \frac{d\omega}{dt} = -\frac{3J_2n_0r_E^2(2-2.5\sin^2 i_0)}{2a_0^2} \end{cases} \quad (4)$$

where r_E is the mean equator radius.

Note that according to Eq. (2) and Eq. (3), when calculating the effects of thrust and perturbations, we assumed the orbit is circular. The bias of this assumption can be evaluated by the terms in Eq. (1) that include e and p . Assume $e = 0.1$ (for most near-circular satellites in LEO), then, $p = 0.99a$ and the gap can be ignored. Meanwhile, the maximum error of $e \cos f$ and $e \sin f$ is 10% and the accumulate error would be much less after an integral from 0 to 2π . The impulsive trajectory optimization in (Huang et al., 2020) used the same assumption and the simulation indicated that although the eccentricity difference is a little greater than 0.1, the relative error is less than 5%. Moreover, we will also provide iteration process in the next section to correct the law of thrust and eliminate the deviations of terminal states. Therefore, the assumption would be reasonable and applicable for most cases in LEO.

(2) Second, as illustrated in Fig.1, $c(u)$, α_n , α_t , and α_r are defined as in Eqs. (5) and (6), when η, k_1, k_2, u, β , and ϕ are given.

$$c(u) = \begin{cases} 1, & \text{if } u \in [-\frac{k_1\pi}{2} + u_1, \frac{k_1\pi}{2} + u_1] \\ 1, & \text{if } u \in [-\frac{k_2\pi}{2} + u_1 + \pi, \frac{k_2\pi}{2} + u_1 + \pi] \\ 0, & \text{else} \end{cases} \quad (5)$$

$$\begin{cases} \alpha_t = \begin{cases} \alpha \cos\beta, & \text{if } u \in [-\frac{k_1\pi}{2} + u_1, \frac{k_1\pi}{2} + u_1] \\ \eta\alpha \cos\beta, & \text{if } u \in [-\frac{k_2\pi}{2} + u_1 + \pi, \frac{k_2\pi}{2} + u_1 + \pi] \end{cases} \\ \alpha_n = \begin{cases} \alpha \sin\beta \cos\phi, & \text{if } u \in [-\frac{k_1\pi}{2} + u_1, \frac{k_1\pi}{2} + u_1] \\ -\alpha \sin\beta \cos\phi, & \text{if } u \in [-\frac{k_2\pi}{2} + u_1 + \pi, \frac{k_2\pi}{2} + u_1 + \pi] \end{cases} \\ \alpha_r = \begin{cases} \alpha \sin\beta \sin\phi, & \text{if } u \in [-\frac{k_1\pi}{2} + u_1, \frac{k_1\pi}{2} + u_1] \\ -\alpha \sin\beta \sin\phi, & \text{if } u \in [-\frac{k_2\pi}{2} + u_1 + \pi, \frac{k_2\pi}{2} + u_1 + \pi] \end{cases} \end{cases} \quad (6)$$

where k_1 and k_2 should be positive and $k_1\pi + k_2\pi \leq 2\pi$. Then, according to Eq. (3), the changes in elements after one revolution is the definite integral from 0 to 2π , which is an extension of Eq. (3) in (Huang et al., 2022b) by involving the

eccentricity:

$$\begin{cases} \Delta a = \int_{u_1-k_1\pi/2}^{u_1+k_1\pi/2} da + \int_{u_1+\pi-k_2\pi/2}^{u_1+\pi+k_2\pi/2} da = \frac{a_0\alpha \cos\beta}{V_0} (k_1 + \eta k_2) T \\ \Delta i = \int_{u_1-k_1\pi/2}^{u_1+k_1\pi/2} di + \int_{u_1+\pi-k_2\pi/2}^{u_1+\pi+k_2\pi/2} di = \frac{(k_1k_1^T + k_2k_2^T)\alpha \sin\beta \cos\phi \cos u_1}{2V_0} T \\ \Delta \Omega = \int_{u_1-k_1\pi/2}^{u_1+k_1\pi/2} d\Omega + \int_{u_1+\pi-k_2\pi/2}^{u_1+\pi+k_2\pi/2} d\Omega = \frac{(k_1k_1^T + k_2k_2^T)\alpha \sin\beta \cos\phi \cos u_1}{2V_0 \sin i} T \\ \Delta e_x = \int_{u_1-k_1\pi/2}^{u_1+k_1\pi/2} de_x + \int_{u_1+\pi-k_2\pi/2}^{u_1+\pi+k_2\pi/2} de_x \\ = \left[\frac{(k_1k_1^T - \eta k_2k_2^T)\alpha \cos\beta \cos u_1}{V_0} + \frac{(k_1k_1^T + k_2k_2^T)\alpha \sin\beta \sin\phi \sin u_1}{2V_0} \right] T \\ \Delta e_y = \int_{u_1-k_1\pi/2}^{u_1+k_1\pi/2} de_y + \int_{u_1+\pi-k_2\pi/2}^{u_1+\pi+k_2\pi/2} de_y \\ = \left[\frac{(k_1k_1^T - \eta k_2k_2^T)\alpha \cos\beta \sin u_1}{V_0} - \frac{(k_1k_1^T + k_2k_2^T)\alpha \sin\beta \sin\phi \cos u_1}{2V_0} \right] T \end{cases} \quad (7)$$

where $\alpha = \alpha_{\max}$, $T = \frac{2\pi}{n}$ is the orbit period, $k_1^T = \frac{\sin \frac{\pi k_1}{2}}{\pi k_1/2}$, and $k_2^T = \frac{\sin \frac{\pi k_2}{2}}{\pi k_2/2}$ are the equivalent coefficients of thrust corresponding to k_1 and k_2 .

When the transfer duration is much longer than T , assuming that the orbital elements change at a uniformly average speed is reasonable (Huang et al., 2022b; Casalino, 2014). Thus, orbit changes after a given time Δt can be calculated by replacing T with Δt in Eq. (7).

(3) Third, according to Eq. (4) the changes in the semimajor axis and inclination will lead to accumulative changes in the argument of latitude, the argument of perigee, and RAAN, which can be analytically calculated as follows.

Assuming that Δa and Δi are obtained using Eq. (7) and the

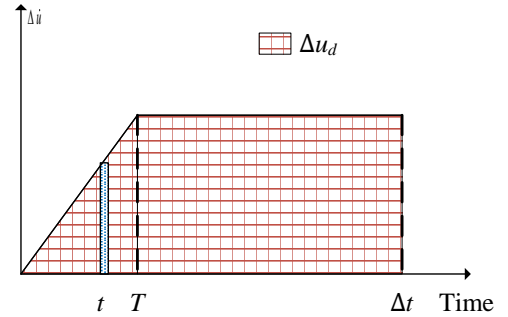


Fig. 2. Drift of argument of latitude.

orbital period is T . Then, the average change rate of a and i are $\dot{a} = \frac{\Delta a}{T}$ and $\dot{i} = \frac{\Delta i}{T}$. Although we assume u moves at a constant velocity n_0 when calculating other orbit elements by Eq. (7), the effect of Δa on u after a long duration must be considered for accurate orbit rendezvous, as illustrated in Fig. 2 ($\Delta \dot{u}$ is the relative drift rate of u compared with the initial orbit). The change in u after a given duration Δt (including T) can be expressed by the definite integral as:

$$\begin{aligned} \Delta u_d &= \int_0^{\Delta t} \Delta \dot{u} dt = \int_0^T \frac{\dot{u}}{da} \dot{a} dt + (\Delta t - T) \frac{\dot{u}}{da} \dot{a} T \\ &= -\frac{3n\dot{a}}{2a} \left(\frac{1}{2} T^2 + (\Delta t - T) T \right) \\ &= -\frac{3n\Delta a}{2a} \left(\Delta t - \frac{1}{2} T \right) \\ &= (n_T - n_0) \left(\Delta t - \frac{1}{2} T \right) \end{aligned} \quad (8)$$

where we assume $\Delta \dot{u} \approx \frac{\dot{u}}{da} \Delta a$. $\frac{\dot{u}}{da} = \frac{dn}{da} = -\frac{3n}{2a}$ represents the derivative of u with respect to semimajor axis. n_0 and n_T are the angular velocities of initial orbit and orbit after one-revolution

control.

Similarly, the change in RAAN after Δt is

$$\begin{aligned} \Delta\Omega_d &= \int_0^{\Delta t} \Delta\dot{\Omega} dt \\ &= \int_0^T \left(\frac{d\dot{\Omega}}{da} \dot{a}t + \frac{d\dot{\Omega}}{di} \dot{i}t \right) dt + (\Delta t - T) \left(\frac{d\dot{\Omega}}{da} \dot{a}T + \frac{d\dot{\Omega}}{di} \dot{i}T \right) \\ &= \left(\frac{d\dot{\Omega}}{da} \dot{a} + \frac{d\dot{\Omega}}{di} \dot{i} \right) \left(\frac{T^2}{2} + \Delta t T - T^2 \right) \\ &= \Delta\dot{\Omega}_T \left(\Delta t - \frac{T}{2} \right) \end{aligned} \quad (9)$$

where we assume $\Delta\dot{\Omega} \approx \frac{d\dot{\Omega}}{da} \Delta a + \frac{d\dot{\Omega}}{di} \Delta i$. $\frac{d\dot{\Omega}}{da}$ and $\frac{d\dot{\Omega}}{di}$ are the derivative of $\dot{\Omega}$ with respect to semimajor axis and inclination by Eq.(4). $\Delta\dot{\Omega}_T = \dot{\Omega}_T - \dot{\Omega}_0$ represents the relative drift rate of RAAN. $\dot{\Omega}_0$ and $\dot{\Omega}_T$ are the RAAN drift rates of initial orbit and the orbit after T , respectively.

The change in ω after Δt is

$$\begin{aligned} \Delta\omega_d &= \int_0^{\Delta t} \Delta\dot{\omega} dt \\ &= \int_0^T \left(\frac{d\dot{\omega}}{da} \dot{a}t + \frac{d\dot{\omega}}{di} \dot{i}t \right) dt + (\Delta t - T) \left(\frac{d\dot{\omega}}{da} \dot{a}T + \frac{d\dot{\omega}}{di} \dot{i}T \right) \\ &= \Delta\dot{\omega}_T \left(\Delta t - \frac{T}{2} \right) \end{aligned} \quad (10)$$

where we assume $\Delta\dot{\omega} \approx \frac{d\dot{\omega}}{da} \Delta a + \frac{d\dot{\omega}}{di} \Delta i$. $\frac{d\dot{\omega}}{da}$ and $\frac{d\dot{\omega}}{di}$ are the derivative of $\dot{\omega}$ with respect to semimajor axis and inclination by Eq.(4). $\Delta\dot{\omega}_T = \dot{\omega}_T - \dot{\omega}_0$ represents the relative drift rate of argument of perigee. $\dot{\omega}_0$ and $\dot{\omega}_T$ are the drift rates of initial orbit and the orbit after T , respectively.

(4) Four, the propellant cost is sufficiently small compared to the spacecraft's mass, thus the fuel-optimal objective function is equal to minimizing the actual time of thrust-on arcs. The length of thrust-on arcs in one revolution is calculated as

$$\Delta t_{thrust} = \frac{(k_1 + k_2)}{2} T \quad (11)$$

3.3. Optimization model

According to Eqs. (3) (11), the terminal constraints $\sigma(t_f) = \sigma_f$ and objective function can be analytically expressed by the 14-dimensional unknowns ($\Delta t_1, \Delta t_2, \eta_1, k_{11}, k_{12}, \beta_1, \phi_1, u_1, \eta_2, k_{21}, k_{22}, \beta_2, \phi_2, u_2$). First, the changes in orbit elements during the first stage Δt_1 (transfer from the initial orbit to the intermediate drift orbit) are small

$$\begin{cases} \Delta a_1 = \frac{\alpha \cos \beta a_0}{V_0} (k_{11} + \eta k_{12}) \Delta t_1 \\ \Delta i_1 = \frac{(k_{11} k_{11}^T + k_{12} k_{12}^T) \alpha \sin \beta_1 \cos \phi_1 \cos u_1}{2V_0} \Delta t_1 \\ \Delta \Omega_1 = \frac{(k_{11} k_{11}^T + k_{12} k_{12}^T) \alpha \sin \beta_1 \cos \phi_1 \sin u_1}{2V_0 \sin i_0} \Delta t_1 \\ \Delta e_{x1} = \left[\frac{(k_{11} k_{11}^T - \eta k_{12} k_{12}^T) \alpha \cos \beta_1 \cos u_1}{V_0} + \frac{(k_{11} k_{11}^T + k_{12} k_{12}^T) \alpha \sin \beta_1 \sin \phi_1 \sin u_1}{2V_0} \right] \Delta t_1 \\ \Delta e_{y1} = \left[\frac{(k_{11} k_{11}^T - \eta k_{12} k_{12}^T) \alpha \cos \beta_1 \sin u_1}{V_0} - \frac{(k_{11} k_{11}^T + k_{12} k_{12}^T) \alpha \sin \beta_1 \sin \phi_1 \cos u_1}{2V_0} \right] \Delta t_1 \end{cases}$$

Similarly, the changes in orbit elements $\Delta a_2, \Delta i_2, \Delta \Omega_2, \Delta e_{x2}, \Delta e_{y2}$ during Δt_2 (transfer from the intermediate drift orbit to the target orbit) can be calculated. To complete the orbit rendezvous, the constraints are:

$$\begin{cases} \Delta a_2 + \Delta a_1 = \Delta a_0 \\ \Delta i_2 + \Delta i_1 = \Delta i_0 \\ \Delta \Omega_2 + \Delta \Omega_1 + \Delta \Omega_d = \Delta \Omega_0 \\ \Delta e_{x2} + \Delta e_{x1}' = \Delta e_{x0} \\ \Delta e_{y2} + \Delta e_{y1}' = \Delta e_{y0} \\ \Delta u_d = \Delta u_0 \end{cases} \quad (13)$$

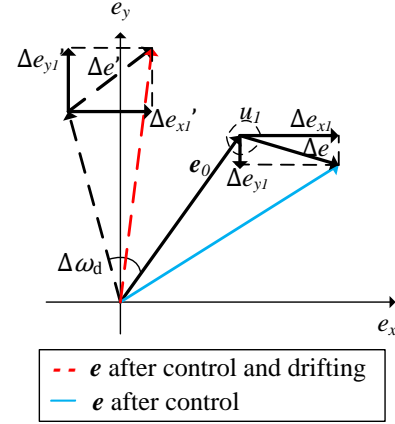


Fig. 3. Drift of eccentricity change.

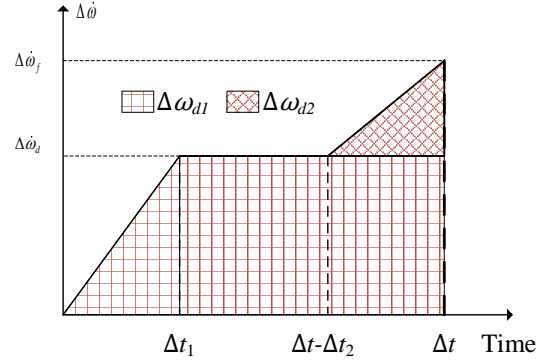


Fig. 4. Calculation of $\Delta\omega_d$.

where $\Delta a_0, \Delta i_0, \Delta \Omega_0, \Delta u_0, \Delta e_{x0}, \Delta e_{y0}$ represent the orbit differences between the initial and target orbit. $\Delta e_{x1}'$ and $\Delta e_{y1}'$ are the corrected changes in eccentricity when considering the drifting of argument of perigee after Δt (as illustrated in Fig. 3):

$$(12) \quad \begin{cases} \Delta e_{x1}' = \left[\frac{(k_{11} k_{11}^T - \eta k_{12} k_{12}^T) \alpha \cos \beta_1 \cos(u_1 + \Delta\omega_d)}{V_0} - \frac{(k_{11} k_{11}^T + k_{12} k_{12}^T) \alpha \sin \beta_1 \sin \phi_1 \sin(u_1 + \Delta\omega_d)}{2V_0} \right] \Delta t_1 \\ \Delta e_{y1}' = \left[\frac{(k_{11} k_{11}^T - \eta k_{12} k_{12}^T) \alpha \cos \beta_1 \sin(u_1 + \Delta\omega_d)}{V_0} - \frac{(k_{11} k_{11}^T + k_{12} k_{12}^T) \alpha \sin \beta_1 \sin \phi_1 \cos(u_1 + \Delta\omega_d)}{2V_0} \right] \Delta t_1 \end{cases} \quad (14)$$

where $\Delta\omega_d$ means the rotate angle of Δe_{x1} and Δe_{y1} from beginning to Δt (as illustrated in Fig. 4) and can be calculated by substituting Δt_1 and Δt_2 to Eq. (10) to replace T and summarizing the results:

$$\begin{aligned} \Delta\omega_d &= \Delta\omega_{d1} + \Delta\omega_{d2} \\ &= (\dot{\omega}_d - \dot{\omega}_0) \left(\Delta t - \frac{\Delta t_1}{2} \right) + (\dot{\omega}_f - \dot{\omega}_d) \left(\Delta t_2 - \frac{\Delta t_2}{2} \right) \end{aligned} \quad (15)$$

where $\dot{\omega}_0, \dot{\omega}_d$, and $\dot{\omega}_f$ are the drift rates of ω of the initial orbit, intermediate orbit, and target orbits. Δe_{x2} and Δe_{y2} do not need to be corrected because the third transfer stage is close to the

rendezvous time and the drift of ω can be ignored.

In the same way as Fig. 3, $\Delta\Omega_d$ in Eq. (13) represents the change in Ω by the perturbation and can be calculated by Eq. (9):

$$\Delta\Omega_d = (\dot{\Omega}_d - \dot{\Omega}_0)(\Delta t - \frac{\Delta t_1}{2}) + (\dot{\Omega}_f - \dot{\Omega}_d)(\Delta t_2 - \frac{\Delta t_2}{2}) \quad (16)$$

where $\dot{\Omega}_0, \dot{\Omega}_d$, and $\dot{\Omega}_f$ are the drift rates of Ω of the initial orbit, intermediate orbit, and target orbits.

In the same way, Δu_d in Eq. (13) represents the change in the argument of latitude caused by the semimajor axis and can be calculated by Eq. (8):

$$\Delta u_d = (n_d - n_0)(\Delta t - \frac{\Delta t_1}{2}) + (n_f - n_d)(\Delta t_2 - \frac{\Delta t_2}{2}) \quad (17)$$

where n_0, n_d , and n_f are the angular velocities of the initial orbit, intermediate orbit, and target orbits, respectively. Since n_d is only determined by Δa_1 (n_d), when $\eta_1, u_1, k_{11}, k_{12}, \beta_1, \phi_1$ are given, Δu_d can be directly calculated by Eq. (17) and may be not equal to Δu_0 . Then, we can always add a correction term to k_{11} by Eq. (18) to ensure $\Delta u_d = \Delta u_0$:

$$\Delta k_{11} = -\frac{2}{3} \frac{\Delta u_0 - \Delta u_d}{\Delta t n_0} \frac{V_0}{\alpha \cos \beta \Delta t_1} \quad (18)$$

where Δk_{11} is the correction to k_{11} . Thus, the constraint of orbit rendezvous on u is automatically satisfied.

The objective function is written as

$$J = \frac{(k_{11} + k_{12})}{2} \Delta t_1 + \frac{(k_{21} + k_{22})}{2} \Delta t_2 \quad (19)$$

Above all, Eqs. (13) to (19) form the optimization model of 14 parameters and 5 constraints. According to the possible values of η_1 and η_2 , there are 4 conditions ($\eta_1 = 1, \eta_2 = 1$; $\eta_1 = -1, \eta_2 = 1$; $\eta_1 = 1, \eta_2 = -1$; and $\eta_1 = -1, \eta_2 = -1$) that can be solved separately and the solution that minimizes J can be chosen as the optimal solution.

3.4. Dimensionality reduction via a sub boundary value problem

Note that $\Delta a_2, \Delta i_2, \Delta \Omega_2, \Delta e_{x2}, \Delta e_{y2}$ can be analytically obtained by Eq. (13) when $\eta_1, u_1, k_{11}, k_{12}, \beta_1, \phi_1$ are given. Meanwhile, $\eta_2, u_2, k_{21}, k_{22}, \beta_2, \phi_2$ and $\Delta a_2, \Delta i_2, \Delta \Omega_2, \Delta e_{x2}, \Delta e_{y2}$ correspond by Eq. (12). Thus, if we can obtain the inverse solution of Eq. (12), the constraint of Eq. (13) can be eliminated from the optimization model and only $\Delta t_1, \Delta t_2, \eta_1, u_1, k_{11}, k_{12}, \beta_1$ and ϕ_1 will be retained as unknown parameters.

Solving $\eta_2, u_2, k_{21}, k_{22}, \beta_2, \phi_2$ by $\Delta a_2, \Delta i_2, \Delta \Omega_2, \Delta e_{x2}, \Delta e_{y2}$ is a boundary value problem like the Lambert's problem. First, u_2 can be directly obtained by Eq. (12):

$$u_2 = \arctan(\Delta\Omega_2 \sin i_0, \Delta i_2) \quad (20)$$

Then, defining C and D as temporary variables, we get:

$$\begin{cases} C = \frac{(k_{21}k_{21}^T - \eta_2 k_{22}k_{22}^T)\alpha \cos \beta_2 \Delta t_2}{V_0} = \Delta e_{x2} \cos u_2 + \Delta e_{y2} \sin u_2 \\ D = \frac{(k_{21}k_{21}^T + k_{22}k_{22}^T)\alpha \sin \beta_2 \sin \phi_2 \Delta t_2}{2V_0} = \Delta e_{x2} \sin u_2 - \Delta e_{y2} \cos u_2 \end{cases} \quad (21)$$

Then, ϕ_2 can be obtained:

$$\phi_2 = \arctan(D, \sqrt{\Delta i_2^2 + \Delta \Omega_2^2 \sin^2 i_0}) \quad (22)$$

To solve $\eta_2, \beta_2, k_{21}, k_{22}$, two conditions are considered, and the best solution will be reserved as the optimal solution:

(1) $\eta_2 = -1$

In this condition, β_2 can be directly obtained by Eq. (21):

$$\beta_2 = \arctan\left(\frac{2D}{\sin \phi_2}, C\right) \quad (23)$$

Thus, the equations of k_{21}, k_{22} in Eq.(21) are

$$\begin{cases} k_{21}k_{21}^T + k_{22}k_{22}^T = \frac{2}{\pi}(\sin \frac{\pi}{2}k_{21} + \sin \frac{\pi}{2}k_{22}) = \frac{CV_0}{\Delta t_2 \alpha \cos \beta_2} = E \\ k_{21} - k_{22} = \frac{\Delta a_2 V_0}{a_0 \Delta t_2 \alpha \cos \beta_2} = F \end{cases} \quad (24)$$

where E and F are temporary variables and Eq. (24) can be rewritten as

$$\begin{aligned} \sin \frac{\pi}{2}k_{21} + \sin \frac{\pi}{2}(k_{21} - F) &= \frac{\pi}{2}E \\ \Rightarrow (1 + \cos \frac{\pi}{2}F) \sin \frac{\pi}{2}k_{21} - \sin \frac{\pi}{2}F \cos \frac{\pi}{2}k_{21} &= \frac{\pi}{2}E \\ \Rightarrow \sin(\frac{\pi}{2}k_{21} - G) &= \frac{\frac{\pi}{2}E}{\sqrt{2+2\cos \frac{\pi}{2}F}} \end{aligned} \quad (25)$$

where $G = \arctan(\sin \frac{\pi}{2}F, 1 + \cos \frac{\pi}{2}F)$ is a temporary variable.

Hence, when $\left| \frac{\frac{\pi}{2}E}{\sqrt{2+2\cos \frac{\pi}{2}F}} \right| > 1$, there is no solution of k_{21} and k_{22} . Otherwise, there are two solutions:

$$\begin{aligned} \frac{\pi}{2}k_{21} &= \arcsin\left(\frac{\frac{\pi}{2}E}{\sqrt{2+2\cos \frac{\pi}{2}F}}\right) + G \\ \frac{\pi}{2}k_{21} &= \pi - \arcsin\left(\frac{\frac{\pi}{2}E}{\sqrt{2+2\cos \frac{\pi}{2}F}}\right) + G \end{aligned} \quad (26)$$

One can calculate the objective function of two solutions and validate the constraint $k_{12} + k_{22} \leq 2$, and then choose the feasible solution that minimizes J .

(2) $\eta_2 = 1$

In this condition, β_2, k_{21} and k_{22} should be solved jointly by Eq.(12) and Eq.(21):

$$\begin{cases} (k_{21}k_{21}^T - k_{12}k_{12}^T) \cos \beta_2 = \frac{CV_0}{\Delta t_2 \alpha} \\ (k_{21}k_{21}^T + k_{12}k_{12}^T) \sin \beta_2 = \frac{2DV_0}{\Delta t_2 \alpha \sin \phi_2} \\ (k_{21} + k_{22}) \cos \beta_2 = \frac{\Delta a_2 V_0}{a_0 \Delta t_2 \alpha} \end{cases} \quad (27)$$

The nonlinear solving package Minpack (Moré et al., 1980) is adopted to solve the equations, and the approximate initial values can be set by four cases:

When $k_{21} \leq 1$ and $k_{22} \leq 1$, one can assume $\sin(\frac{\pi k_{21}}{2}) \approx \frac{\pi k_{21}}{2}$, $\sin(\frac{\pi k_{22}}{2}) \approx \frac{\pi k_{22}}{2}$. Then, Eq.(27) can be simplified and solved as:

$$\begin{cases} (k_{21} - k_{12}) \cos \beta_2 = \frac{CV_0}{\Delta t_2 \alpha} \\ (k_{21} + k_{12}) \sin \beta_2 = \frac{2DV_0}{\Delta t_2 \alpha \sin \phi_2} \\ (k_{21} + k_{22}) \cos \beta_2 = \frac{\Delta a_2 V_0}{a_0 \Delta t_2 \alpha} \\ \beta_2 = \arctan\left(\frac{2DV_0}{\Delta t_2 \alpha \sin \phi_2}, \frac{\Delta a_2 V_0}{a_0 \Delta t_2 \alpha}\right) \\ k_{21} = \frac{\Delta a_2 V_0}{2a_0 \Delta t_2 \alpha \cos \beta_2} + \frac{CV_0}{2\Delta t_2 \alpha} \\ k_{22} = \frac{\Delta a_2 V_0}{2a_0 \Delta t_2 \alpha \cos \beta_2} - \frac{CV_0}{2\Delta t_2 \alpha} \end{cases} \quad (28)$$

When $k_{21} > 1$ and $k_{22} \leq 1$, one can assume $\sin(\frac{\pi k_{21}}{2}) \approx \frac{\pi(2-k_{21})}{2}$, $\sin(\frac{\pi k_{22}}{2}) \approx \frac{\pi k_{22}}{2}$. Then, Eq.(27) can be simplified and solved as:

$$\begin{cases} (2 - k_{21} - k_{12}) \cos \beta_2 = \frac{CV_0}{\Delta t_2 \alpha} \\ (2 - k_{21} + k_{12}) \sin \beta_2 = \frac{2DV_0}{\Delta t_2 \alpha \sin \phi_2} \Rightarrow \\ (k_{21} + k_{22}) \cos \beta_2 = \frac{\Delta a_2 V_0}{a_0 \Delta t_2 \alpha} \\ \beta_2 = \arccos\left(\frac{CV_0}{2\Delta t_2 \alpha} + \frac{\Delta a_2 V_0}{2a_0 \Delta t_2 \alpha}\right) \\ k_{21} = \left(\frac{\Delta a_2 V_0}{a_0 \Delta t_2 \alpha \cos \beta_2} + 2 - \frac{2DV_0}{\Delta t_2 \alpha \sin \alpha_2 \sin \beta_2}\right)/2 \\ k_{22} = \left(\frac{\Delta a_2 V_0}{a_0 \Delta t_2 \alpha \cos \beta_2} - 2 + \frac{2DV_0}{\Delta t_2 \alpha \sin \alpha_2 \sin \beta_2}\right)/2 \end{cases} \quad (29)$$

When $k_{21} \leq 1$ and $k_{22} > 1$, one can assume $\sin(\frac{\pi k_{21}}{2}) \approx \frac{\pi k_{21}}{2}$, $\sin(\frac{\pi k_{22}}{2}) \approx \frac{\pi(2-k_{22})}{2}$. Then, Eq.(27) can be simplified and solved as:

$$\begin{cases} (2 - k_{21} - 2 + k_{12}) \cos \beta_2 = \frac{CV_0}{\Delta t_2 \alpha} \\ (2 - k_{21} + 2 - k_{12}) \sin \beta_2 = \frac{2DV_0}{\Delta t_2 \alpha \sin \phi_2} \Rightarrow \\ (k_{21} + k_{22}) \cos \beta_2 = \frac{\Delta a_2 V_0}{a_0 \Delta t_2 \alpha} \\ \beta_2 = \arccos\left(-\frac{CV_0}{2\Delta t_2 \alpha} - \frac{\Delta a_2 V_0}{2a_0 \Delta t_2 \alpha}\right) \\ k_{21} = \left(\frac{\Delta a_2 V_0}{a_0 \Delta t_2 \alpha \cos \beta_2} + \frac{\Delta t_2 \alpha \sin \alpha_2 \sin \beta_2}{2DV_0} - 2\right)/2 \\ k_{22} = \left(\frac{\Delta a_2 V_0}{a_0 \Delta t_2 \alpha \cos \beta_2} - \frac{\Delta t_2 \alpha \sin \alpha_2 \sin \beta_2}{2DV_0} + 2\right)/2 \end{cases} \quad (30)$$

When $k_{21} > 1$ and $k_{21} > 1$, $k_{21} + k_{22} > 2$ cannot be satisfied and there is no solution for this case.

Eq. (28), Eq. (29), and Eq. (30) can be used as initial values to solve β_2 , k_{21} and k_{22} separately. Further, the constraints on k_{21} and k_{22} should be validated, and the feasible solution that minimizes J will be retained.

Above all, the solving process from Δa_2 , Δi_2 , $\Delta \Omega_2$, Δe_{x2} , Δe_{y2} to η_2 , u_2 , k_{21} , k_{22} , β_2 , ϕ_2 is obtained. If there is no feasible solution obtained after this process, the given Δa_2 , Δi_2 , $\Delta \Omega_2$, Δe_{x2} , Δe_{y2} are out of the reachable domain of low-thrust, and a punish term should be added to the objective function (Eq. (18)).

3.5. Optimization and parameters correction

After applying the algorithm in Section III.D, there are 8 unknowns. Differential evolution (DE) algorithm (Price et al., 2005) can be used to solve this optimization problem. DE is an efficient evolutionary algorithm for the optimization of continuous variables. Details of DE are beyond the scope of the study and one can refer to (Price et al., 2005). The process is illustrated in Fig. 5.

It should be noted that due to the approximations in the optimization model if we substitute the optimal law of thrust in the numerical dynamic model (Eq. (1), Eq. (5) and Eq. (6)), there may be errors between given target orbit and the predicted orbit after control. Let Δa_p , Δe_{xp} , Δe_{yp} , Δi_p , $\Delta \Omega_p$, Δu_p denote the numerical errors of semimajor axis, eccentricity (two dimensions), inclination, RAAN and argument of latitude, an correction to the solution obtained by DE is proposed as follows. We first calculate the analytical corrections to the changes in orbit elements (Δa_1 , Δe_{x1} , Δe_{y1} , Δi_1 , $\Delta \Omega_1$, and Δa_2 , Δe_{x2} , Δe_{y2} , Δi_2 , $\Delta \Omega_2$) and then update the parameters of thrust (η_1 , u_1 , k_{11} , k_{12} , β_1 , ϕ_1 and η_2 , u_2 , k_{21} , k_{22} , β_2 , ϕ_2) by Eqs. (19) to (30), respectively.

First, let Δa_1^c and Δa_2^c denote the corrections to Δa_1 and Δa_2 . According to Eq. (13) and (17), we can obtain:

$$\begin{cases} \Delta a_1^c + \Delta a_2^c = \Delta a_{1p} \\ -\frac{3n_0}{2a_0} \Delta a_1^c \left(\Delta t - \frac{\Delta t_1}{2}\right) - \frac{3n_0}{2a_0} \Delta a_2^c \left(\Delta t_2 - \frac{\Delta t_2}{2}\right) = \Delta u_p \end{cases} \quad (31)$$

where $-\frac{3n_0}{2a_0} \Delta a_1^c$ and $-\frac{3n_0}{2a_0} \Delta a_2^c$ are changes in angular velocity by Δa_1^c and Δa_2^c . Then, Δa_1^c and Δa_2^c can be solved by Eq.(31):

$$\begin{cases} \Delta a_1^c = \frac{\frac{\Delta t_2}{2} \Delta a_{1p} + \frac{2a_0 \Delta u_p}{3n_0}}{(\Delta t_2 - \Delta t)} \\ \Delta a_2^c = \Delta a_{1p} - \Delta a_1^c \end{cases} \quad (32)$$

Second, let Δi_1^c and Δi_2^c denote the correction to Δi_1 and Δi_2 . u_1 and u_2 are assumed unchanged after the correction, which is more convenient to derive analytical equations of Δi_1^c and Δi_2^c (Huang et al., 2022b). According to Eq. (13) and (17), we can obtain:

$$\begin{cases} \Delta i_1^c + \Delta i_2^c = \Delta i_p \\ \Delta \Omega_1^c + \Delta \Omega_2^c + \dot{\Omega}_0 \left(-3.5 \frac{\Delta a_1^c}{a_0} - \tan i_0 \Delta i_1^c\right) \left(\Delta t - \frac{\Delta t_1}{2}\right) \\ + \dot{\Omega}_0 \left(-3.5 \frac{\Delta a_2^c}{a_0} - \tan i_0 \Delta i_2^c\right) \left(\frac{\Delta t_2}{2}\right) = \Delta \Omega_p \end{cases} \quad (33)$$

where $\dot{\Omega}_0 \left(-3.5 \frac{\Delta a_1^c}{a_0} - \tan i_0 \Delta i_1^c\right)$ and $\dot{\Omega}_0 \left(-3.5 \frac{\Delta a_2^c}{a_0} - \tan i_0 \Delta i_2^c\right)$ means the changes in RAAN caused by the corrections to semi-major axis and inclination. Because $\Delta \Omega_1^c$ and $\Delta \Omega_2^c$ can be expressed by $\frac{\tan u_1}{\sin i_0} \Delta i_1^c$ and $\frac{\tan u_2}{\sin i_0} \Delta i_2^c$, Eq.(33) can be transformed to binary linear equations of Δi_1^c and Δi_2^c , and can be solved as:

$$\begin{cases} \Delta i_1^c + \Delta i_2^c = \Delta i_p \\ \frac{\tan u_1}{\sin i_0} \Delta i_1^c + \frac{\tan u_2}{\sin i_0} \Delta i_2^c = S \Rightarrow \begin{cases} \Delta i_1^c = \frac{R \Delta i_p - S}{R - Q} \\ \Delta i_2^c = \Delta i_p - \Delta i_1^c \end{cases} \end{cases} \quad (34)$$

where Q, R and S are temporary variables:

$$\begin{cases} Q = \left(\frac{\tan u_1}{\sin i_0} - \tan i_0 \dot{\Omega}_0 \left(\Delta t - \frac{\Delta t_1}{2}\right)\right) \\ R = \left(\frac{\tan u_2}{\sin i_0} - \tan i_0 \dot{\Omega}_0 \frac{\Delta t_2}{2}\right) \\ S = \Delta \Omega_p + \dot{\Omega}_0 \left(3.5 \frac{\Delta a_1^c}{a_0}\right) \left(\Delta t - \frac{\Delta t_1}{2}\right) + \dot{\Omega}_0 \left(3.5 \frac{\Delta a_2^c}{a_0}\right) \left(\frac{\Delta t_2}{2}\right) \end{cases} \quad (35)$$

Thus, $\Delta \Omega_1^c$ and $\Delta \Omega_2^c$ are also obtained.

Third, divide Δe_{xp} and Δe_{yp} into two parts as the corrections to Δe_{x1} , Δe_{y1} , Δe_{x2} and Δe_{y2} according to the ratio of thrust time in the first and third stages:

$$\begin{cases} \Delta e_{x1}^c = \chi \Delta e_{xp} \\ \Delta e_{y1}^c = \chi \Delta e_{yp} \\ \Delta e_{x2}^c = (1 - \chi) \Delta e_{xp} \\ \Delta e_{y2}^c = (1 - \chi) \Delta e_{yp} \end{cases} \quad (36)$$

where the superscript 'c' represents correction term and $\chi = \frac{|k_{11}| + |k_{12}|}{|k_{11}| + |k_{12}| + |k_{21}| + |k_{22}|}$ represents the ratio of thrust time in the first transfer stage and total thrust time. Eq. (36) means the corrections of numerical eccentricity error that approximately allocated to the first and third transfer stage are proportionate to their thrust time. Note that the correction to Δe_{x1} and Δe_{y1} should consider the natural drift of argument of perigee during the transfer. Therefore, according to Fig. 3, Δe_{x1} and Δe_{y1} should be recalculated to correct the drift angle $\Delta \omega_d$ by Eq.

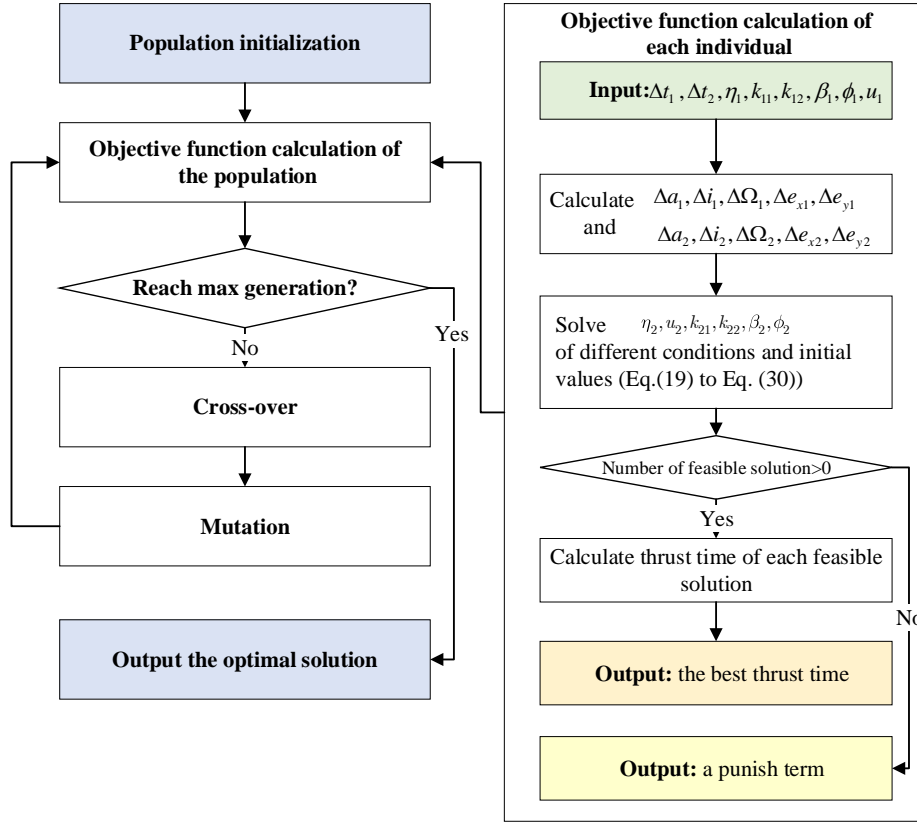


Fig. 5. Flowchart of the optimization process.

(15):

$$\begin{cases} u_1^c = \arctan(\Delta e_{y1}^c, \Delta e_{x1}^c) \\ \Delta e_1^c = \sqrt{(\Delta e_{x1}^c)^2 + (\Delta e_{y1}^c)^2} \\ \Delta e_{x1}^c = \Delta e_1^c \cos(u_1^c - \Delta \omega_d) \\ \Delta e_{y1}^c = \Delta e_1^c \sin(u_1^c - \Delta \omega_d) \end{cases} \quad (37)$$

where u_1^c is the argument of latitude of the eccentricity correction and Δe_1^c is the magnitude.

Above all, $\Delta a_1, \Delta i_1, \Delta \Omega_1, \Delta e_{x1}, \Delta e_{y1}$ and $\Delta a_2, \Delta i_2, \Delta \Omega_2, \Delta e_{x2}, \Delta e_{y2}$ have been correct and the parameters $\eta_1, u_1, \beta_1, \phi_1, k_{11}, k_{12}$ and $\eta_2, u_2, \beta_2, \phi_2, k_{21}, k_{22}$ can be updated by solving Eqs. (20)–(30), respectively. The correction process can be repeated multiple times to obtain high-precision trajectory. The flow chart is illustrated in Fig. 6.

4. Simulation Result

In this study, a transfer between two space debris is analyzed. The initial and target orbits of the spacecraft are listed in Table 1. The transfer duration is 20 days and the constant acceleration is $6 \times 10^{-4} m/s^2$. The population of DE is set to 50, and the max generation is 800. Meanwhile, the crossover operator is 'Ran2Bestexp' (Price et al., 2005) with a probability of 0.8 and the mutation probability is set to 0.8.

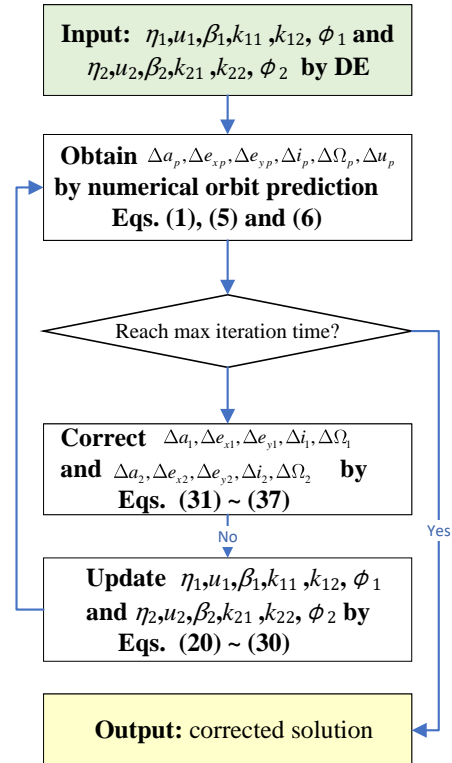


Fig. 6. Flowchart of the correction process.

Table 1. Detail of orbits

	Orbit	$a(m)$	e	i (deg)	Ω (deg)	ω (deg)	M (deg)
Initial	Mean	7157398	0.01521	98.6435	152.508	20.285	341.629
	Osculating	7166678	0.01566	98.637	152.507	19.818	342.100
Target	Mean	7111954	0.00721	97.4512	151.175	44.985	59.376
	Osculating	7103971	0.00678	97.455	151.178	32.638	71.695

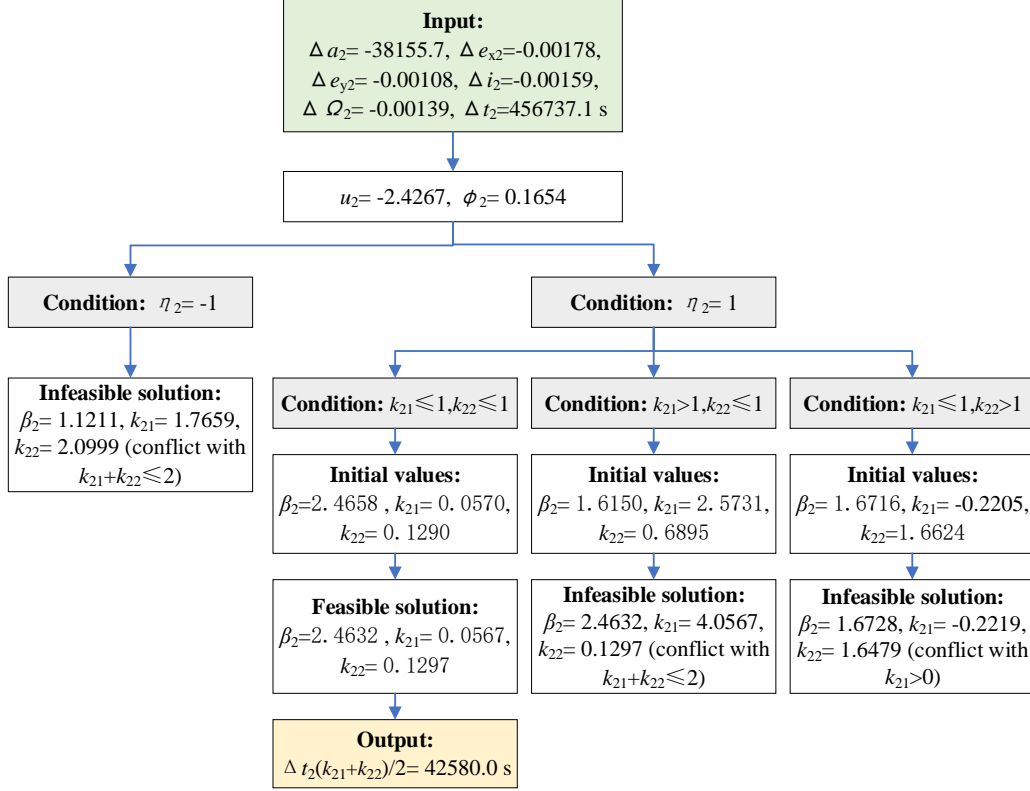


Fig. 7. Process of the sub boundary value problem.

4.1. Optimal solution

The optimal $\Delta t_1, \Delta t_2, \eta_1, u_1, \beta_1, \alpha_1, k_{11}, k_{12}, \eta_2, u_2, \beta_2, \phi_2, k_{21}$, and k_{22} obtained by DE are [7.8908, 5.2863, -1, -2.7460, 1.3779, 0.0141, 0.3691, 0.4660, 1, -2.4267, 2.4632, 0.1654, 0.0567, 0.1297]. The total length of thrust-on arcs is 3.78 days, and the equivalent velocity increment is 196.35 m/s. The calculation takes less than 2 s on a personal computer (CPU: AMD Ryzen7 4.2 GHz).

The process of the sub boundary value problem in Section III.D corresponding to the optimal solution is illustrated in Fig.7. In summary, the algorithm can correctly check the low-thrust reachability and quickly obtain $\eta_2, u_2, \beta_2, \phi_2, k_{21}, k_{22}$ by given $\Delta a_2, \Delta i_2, \Delta \Omega_2, \Delta e_{x2}, \Delta e_{y2}$. Repeating calculations proved that less than 20 shootings are required for Minpack to solve Eq. (27) with initial values by Eqs. (28-30).

The errors after each correction step are also detailed in Table 2. After five steps, the errors are close to zero and can be ignored (the position error is less than 10 m and the velocity error is less than 0.03 m/s). Finally the optimal 14 parameters are [7.8908, 5.2863, -1, -2.7473, 1.3809, 0.0906, 0.3748, 0.4650, 1, -2.4307, 2.4632, 0.1846, 0.0636, 0.1239]. The optimal thrust is

illustrated in Fig. 8. Differing from the symmetrical thrust strategy in (Huang et al., 2022b), the lengths of two thrust-on arcs in each revolution are not the same to make use of the tangential acceleration to change eccentricity. The history of the orbit elements is illustrated in Fig. 9, which indicates that the optimal law of thrust firstly should partly decrease the semimajor axis and inclination to achieve the optimal drift rates of RAAN and the argument of perigee. Finally, after a long duration of natural drift, the thrust is employed again to control the spacecraft to rendezvous with the target orbit. The equivalent velocity increment (197.48 m/s) is very close to the minimum velocity increment (196.10 m/s) obtained by the indirect method (Jiang et al., 2012; Li et al., 2018; Zhao et al., 2017) after multiple calculations (repeating with different randomly generated co-states to obtain the global optimal solution), which proved the optimality of the proposed method.

4.2. Analysis of different thrust accelerations

To validate the applicability of the proposed method for different thrust levels, four cases of thrust acceleration ($1 \times$

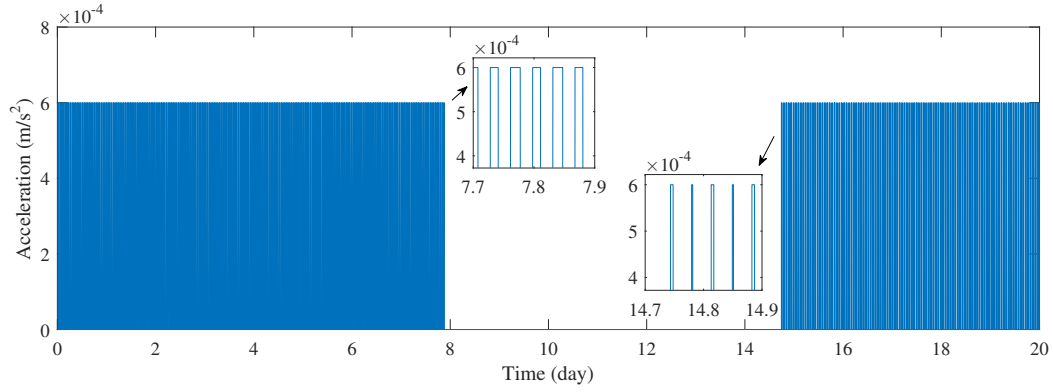


Fig. 8. Fuel-optimal law of thrust.

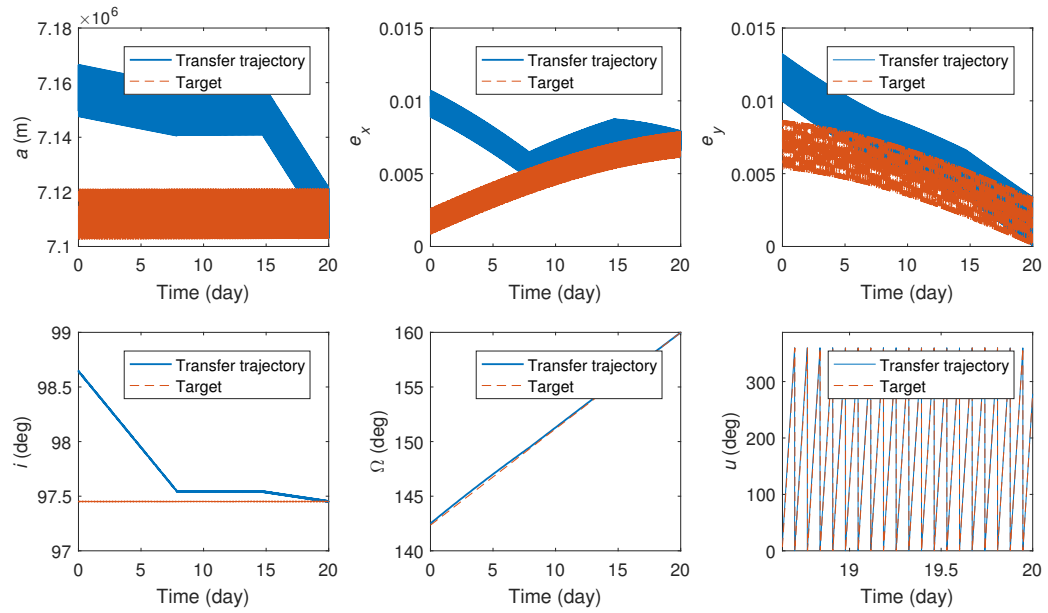


Fig. 9. History of orbit elements during the transfer.

Table 2. Numerical errors of orbit elements

Step	$\Delta a_p(m)$	Δe_{xp}	Δe_{yp}	$\Delta i_p(deg)$	$\Delta \Omega_p(deg)$	$\Delta u_p(deg)$
0	489.1315	-0.0035	-0.0089	-12.2485	0.00105	0.00163
1	-94.4675	0.00043	0.01118	1.5021	0.000261	-0.00011
2	-18.1261	-9.47E-05	-0.00149	0.2739	-8.58E-06	-3.85E-05
3	1.76396	-1.21E-05	4.21E-06	-0.0371	-5.76E-06	5.23E-07
4	0.45304	2.02E-06	3.69E-05	-0.0093	-7.10E-08	7.79E-07
5	0.01925	7.73E-07	1.81E-06	-2.36E-04	1.09E-07	1.73E-08

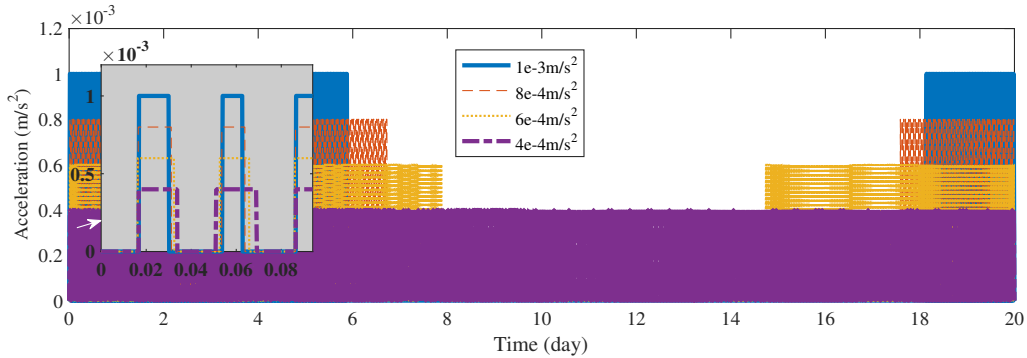


Fig. 10. Law of thrust of different accelerations.

$10^{-3}m/s^2$, $8 \times 10^{-4}m/s^2$, $6 \times 10^{-4}m/s^2$, $4 \times 10^{-4}m/s^2$) are tested and the law of thrust are illustrated in Fig.10. When the thrust acceleration is larger, the optimal solution prefers longer natural drift duration to save fuel because the spacecraft can be transferred to the drift orbit faster. When the thrust acceleration is smaller, it's more difficult to transfer to the drift orbit and thus larger velocity increment is required for direct non-coplanar control. However, it can be seen that coast arcs in the transfers arriving and departing the drift orbit are usually necessary to save propellant. It's also obtained that the orbit transfer problem in Table 1 will be infeasible when the acceleration is smaller than $2.7 \times 10^{-4}m/s^2$.

The equivalent velocity increments of different transfer durations and different thrust accelerations are illustrated in Fig.11, which indicates the natural drift of RAAN and argument of perigee can greatly decrease the propellant when the transfer duration is long enough. The method in this paper can well adept with trajectory optimization of different conditions. Optimization by DE could ensure the thrust parameters achieve the balance between direct control of orbit elements and indirect control via natural drift.

4.3. Comparison with previous methods and discussion

In this study, the thrust strategy is just approximately optimal because the direction of thrust acceleration is fixed and the thrust keeps the same in different revolutions. However, the solutions obtained from repeated calculations are consistent and are proved to be always very close to the best results of the indirect methods with numerical dynamics (Jiang et al., 2012; Li et al., 2018; Zhao et al., 2017) after a lot of simulations with different orbits and transfer durations. By contrast, the methods

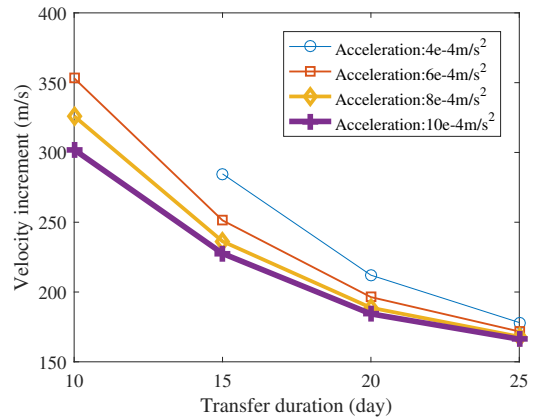


Fig. 11. Velocity increment of different transfer duration and acceleration.

in (Jiang et al., 2012; Li et al., 2018; Zhao et al., 2017) may easily converge to locally optimal solutions when solving such long-duration perturbed orbit rendezvous problems because the number of revolutions is large and the effect of perturbations cannot be globally considered. Fig. 12 shows examples of several local optimal solutions ($\Delta t = 10$ days) obtained by an indirect method corresponding to very large velocity increments.

The approximate methods in (Huang et al., 2022a; Cerf, 2016; Wen et al., 2021; Huang et al., 2022b) are also tested using the same orbits in Table 1 with different transfer durations and different thrust accelerations. Taking the best results of the indirect method as a benchmark, the comparisons of precision and efficiency between different methods (using the same computer) are detailed in Table 3, which demonstrates the performance of

Table 3. Comparison of different methods

Method	Calculation time (s)	Maximum relative error
This study	2	3.5%
Numerical method in (Jiang et al., 2012; Li et al., 2018; Zhao et al., 2017)	>14400	Used as benchmark
Approximate iteration method in (Huang et al., 2022a)	0.01	7.9%
Approximate methods (Cerf, 2016; Wen et al., 2021; Huang et al., 2022b)	1	Only for circular orbits

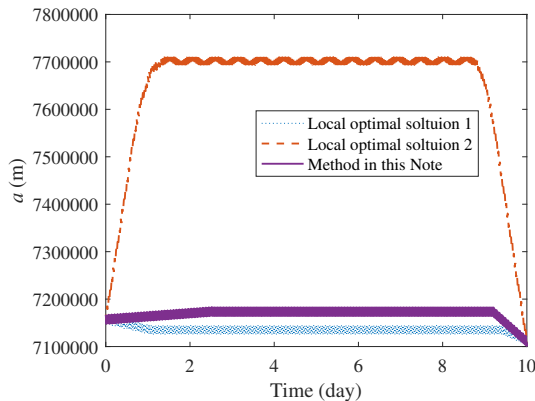


Fig. 12. Velocity increment of different transfer duration and acceleration.

the proposed method. For the case in Table 1, the relative errors of methods in (Cerf, 2016; Wen et al., 2021; Huang et al., 2022b) are greater than 30% because the eccentricity difference is about 0.01, which requires additional velocity increment for orbit rendezvous. The calculation of the proposed method is much less than existing indirect methods requiring hundreds of shooting processes and the thrust law is also much simpler for engineering practice. Besides, the results are also closer to the global optimal solution than existing approximate methods.

5. Conclusion

A priori fuel-optimal thrust strategy is proposed to simplify the trajectory optimization of orbit rendezvous with low eccentricities into a parametric optimization problem, which significantly reduces the solving complexity. By parameterizing the switch strategy and direction of the thrust, the analytical expression of the rendezvous constraint and objective function are obtained and thus a sub boundary value problem is introduced to further reduce the number of unknowns. Finally, a differential evolution algorithm is adopted to solve the simplified optimization model and an analytical correction process is proposed to eliminate the numerical errors. Simulation results and comparisons with previous methods proved this new method's efficiency and high precision for low-eccentricity orbits. The method can be well applied to preliminary analysis and high-precision trajectory optimization of missions such as in-orbit service and active debris removal in low Earth orbits.

6. Acknowledgment

This work was supported by the National Natural Science Foundation of China (No. 12002394 and No. 12172382).

References

- Barea, A., Urrutxua, H., & Cadarso, L. (2022). Relative-inclination strategy for j2-perturbed low-thrust transfers between circular orbits. *J. Guid. Control Dyn.*, 45(10), 1973–1979.
- Berend, N., & Olive, X. (2016). Bi-objective optimization of a multiple-target active debris removal mission. *Acta Astronaut.*, 122, 324–335.
- Bonnal, C., Ruault, J. M., & Desjean, M. C. (2013). Active debris removal: Recent progress and current trends. *Acta Astronaut.*, 85, 51–60.
- Casalino, L. (2014). Approximate optimization of low-thrust transfers between low-eccentricity close orbits. *J. Guid. Control Dyn.*, 37(3), 1003–1008.
- Casalino, L., & Forestieri, A. (2022). Approximate optimal leo transfers with j2 perturbation and dragsail. *Acta Astronaut.*, 192, 379–389.
- Cerf, M. (2014). Multiple space debris collecting mission – optimal mission planning. *J. Optimiz Theory App.*, 167(1), 195–218.
- Cerf, M. (2016). Low-thrust transfer between circular orbits using natural precession. *J. Guid. Control Dyn.*, 39(10), 2232–2239.
- Edelbaum, T. (2003). Optimum low-thrust rendezvous and station keeping. *J. Spacecraft Rockets*, 40(6), 960–965.
- Gao, Y. (2007). Near-optimal very low-thrust earth-orbit transfers and guidance schemes. *J. Guid. Control Dyn.*, 30(2), 12–20.
- Guo, C. M., Zhang, J., Luo, Y. Z. et al. (2018). Phase-matching homotopic method for indirect optimization of long-duration low-thrust trajectories. *Adv. Space Res.*, 62(3), 568–579.
- Huang, A., Luo, Y. Z., & Li, H. N. (2020). Fast estimation of perturbed impulsive rendezvous via semi-analytical equality-constrained optimization. *J. Guid. Control Dyn.*, 43(12), 2383–2390.
- Huang, A., Luo, Y. Z., & Li, H. N. (2022a). Optimization of low-thrust multi-debris removal mission via an efficient approximation model of orbit rendezvous. *P I Mech Eng G-J Aer, Article in advance*(1).
- Huang, A., Luo, Y. Z., & Li, H. N. (2022b). Optimization of low-thrust rendezvous between circular orbits via thrust-switch strategy. *J. Guid. Control Dyn.*, 45(6), 1143–1152.
- Jiang, F., Baoyin, H., & Li, J. (2012). Practical techniques for low-thrust trajectory optimization with homotopic approach. *J. Guid. Control Dyn.*, 35(1), 245–257.
- Kelchner, M., & Kluever, C. (2020). Rapid evaluation of low-thrust transfers from elliptical orbits to geostationary orbit. *J. Spacecraft Rockets*, 57(5), 1–9.
- Leomanni, M., Bianchini, G., Garulli, A. et al. (2020). Orbit control techniques for space debris removal missions using electric propulsion. *J. Guid. Control Dyn.*, 43(7), 1259–1268.
- Li, H., C. S. Y., & Baoyin, H. (2018). J2-perturbed multitarget rendezvous optimization with low thrust. *J. Guid. Control Dyn.*, 41(3), 802–808.
- Moghaddam, B. M., & Chhabra, R. (2021). On the guidance, navigation and control of in-orbit space robotic missions: A survey and prospective vision. *Acta Astronaut.*, 184, 70–100.
- Moré, J., Garbow, B. S., Hillstom, K. E. et al. (1980). User guide for minpack-1. *J. Coll Gen Pract.*
- Neves, R., & Sanchez, J. P. (2020). Low-thrust trajectory design in low-energy regimes using variational equations. *Adv. Space Res.*, 66(9), 2215–2231.
- P, G. (2004). Analysis of j2-perturbed motion using mean non-osculating orbital elements. *Celest Mech Dyn Astr.*, 90(3), 289–306.
- Pontani, M., & Pustorino, M. (2021). Nonlinear earth orbit control using low-thrust propulsion. *Acta Astronaut.*, 179, 296–310.

- Price, K., Storn, R. M., & Lampinen, J. A. (2005). *Differential Evolution: A Practical Approach to Global Optimization (Natural Computing Series)*. Berlin, Heidelberg: Springer-Verlag.
- Ruggiero, A., Pergola, P., & Andrenucci, M. (2015). Small electric propulsion platform for active space debris removal. *IEEE Trans. Plasma Sci*, 43(12), 4200–4209.
- Shen, H., & Tsiotras, P. (2005). Peer-to-peer refueling for circular satellite constellations. *J. Guid. Control Dyn*, 28(6), 1220–1230.
- Shen, H. X. (2021). Explicit approximation for J_2 -perturbed low-thrust transfers between circular orbits. *J. Guid. Control Dyn*, 44(8), 1525–1531.
- Tarzi, Z., Speyer, J., & Wirz, R. (2013). Fuel optimum low-thrust elliptic transfer using numerical averaging. *Acta Astronaut*, 30, 85–118.
- Vallado, D. (2007). *Fundamentals of Astrodynamics and Applications*. New York: Springer New York.
- Wen, C. X., Zhang, C., & Qiao, D. (2021). Low-thrust transfer between circular orbits using natural precession and yaw switch steering. *J. Guid. Control Dyn*, 44(7), 1371–1378.
- Zhao, S., Zhang, J., Xiang, K. et al. (2017). Target sequence optimization for multiple debris rendezvous using low thrust based on characteristics of sso. *Astrodynamics*, 1(1), 15.